

The Analog Data Assimilation

REDOUANE LGUENSAT AND PIERRE TANDEO

IMT Atlantique, Lab-STICC, Université Bretagne Loire, Brest, France

PIERRE AILLIOT

Laboratoire de Mathématiques de Bretagne Atlantique, University of Western Brittany, Brest, France

MANUEL PULIDO

Department of Physics, Universidad Nacional del Nordeste, and CONICET, Corrientes, Argentina

RONAN FABLET

IMT Atlantique, Lab-STICC, Université Bretagne Loire, Brest, France

(Manuscript received 23 November 2016, in final form 31 July 2017)


ABSTRACT

In light of growing interest in data-driven methods for oceanic, atmospheric, and climate sciences, this work focuses on the field of data assimilation and presents the analog data assimilation (AnDA). The proposed framework produces a reconstruction of the system dynamics in a fully data-driven manner where no explicit knowledge of the dynamical model is required. Instead, a representative catalog of trajectories of the system is assumed to be available. Based on this catalog, the analog data assimilation combines the nonparametric sampling of the dynamics using analog forecasting methods with ensemble-based assimilation techniques. This study explores different analog forecasting strategies and derives both ensemble Kalman and particle filtering versions of the proposed analog data assimilation approach. Numerical experiments are examined for two chaotic dynamical systems: the Lorenz-63 and Lorenz-96 systems. The performance of the analog data assimilation is discussed with respect to classical model-driven assimilation. A Matlab toolbox and Python library of the AnDA are provided to help further research building upon the present findings.

1. Introduction

The reconstruction of the spatiotemporal dynamics of geophysical systems from noisy and/or partial observations is a major issue in geosciences. Variational and stochastic data assimilation schemes are the two main categories of methods considered to address this issue [see Evensen (2007) for more details]. A key feature of these data assimilation schemes is that they rely on repeated forward integrations of an explicitly known dynamical model. This may greatly limit their application

range as well as their computational efficiency. First, thorough and time-consuming simulations may be required to identify explicit representations of the dynamics, especially regarding finescale effects and subgrid-scale processes as for instance in regional geophysical models (Hong and Dudhia 2012). Such processes typically involve highly nonlinear and local effects (Wilby and Wigley 1997). The resulting numerical models may be computationally intensive and even prohibitive for assimilation problems, for instance regarding the time integration of members with different initial conditions at each time step. Second, as explained in Van Leeuwen (2010), “with ever-increasing resolution and complexity, the numerical models tend to be highly nonlinear and also observations become more complicated and their relation to the models more nonlinear” (p. 1991). In such situations, standard data assimilation techniques may find difficulties, including

 Supplemental information related to this paper is available at the Journals Online website: <https://doi.org/10.1175/MWR-D-16-0441.s1>.

Corresponding author: Redouane Lguensat, redouane.lguensat@imt-atlantique.fr

DOI: 10.1175/MWR-D-16-0441.1

© 2017 American Meteorological Society. For information regarding reuse of this content and general copyright information, consult the [AMS Copyright Policy](https://www.ametsoc.org/PUBSReuseLicenses) (www.ametsoc.org/PUBSReuseLicenses).

nonlinear particle filters which are prone to the “curse of dimensionality.” Third, difficulties may occur when geophysical dynamics involve uncertain model parameterizations or space–time switching between different dynamical modes that need to be estimated online (Ruiz et al. 2013) or offline (Tandeo et al. 2015b). Dealing with such situations may not be straightforward using classical model-driven assimilation schemes.

Meanwhile, recent years have witnessed a proliferation of satellite data, in situ monitoring, as well as numerical simulations. Large databases of valuable information have been collected and offer a major opportunity for oceanic, atmospheric, and climate sciences. As pioneered by Lorenz (1969), the availability of such datasets advocates for the development of analog forecasting strategies, which make use of “similar” states of the dynamical system of interest to generate realistic forecasts. Analog forecasting strategies have become more and more popular in oceanic and atmospheric sciences (Nagarajan et al. 2015; McDermott and Wikle 2016), and have benefited from recent advances in machine learning (Zhao and Giannakis 2014). They have been applied to a variety of systems and application domains, including among others, rainfall nowcasting (Atencia and Zawadzki 2015), air quality analysis (Delle Monache et al. 2014), wind field downscaling (He-Guelton et al. 2015), climate reconstruction (Schenk and Zorita 2012), and stochastic weather generators (Yiou 2014).

In this work, we examine the extension of the analog forecasting paradigm for data assimilation issues. Given a representative dataset of the dynamics of the system, this extension that we call analog data assimilation (AnDA) consists of a combination of the implicit analog forecasting of the dynamics with stochastic filtering schemes, namely, ensemble Kalman and particle filtering schemes (Evensen and Van Leeuwen 2000). This idea was first introduced in Tandeo et al. (2015a) where the relevance of the proposed analog data assimilation is shown for the reconstruction of complex dynamics from partial and noisy observations. Tandeo et al. derived filtering and smoothing algorithms called the *analog ensemble Kalman filter and smoother*, which combine analog forecasting and the ensemble Kalman filter and smoother. A similar philosophy was followed independently in Hamilton et al. (2016) where the authors combine ideas from Takens’s embedding theorem and ensemble Kalman filtering to infer the hidden dynamics from noisy observations. Hamilton et al. called their algorithm the *Kalman–Takens filter*.

Whereas these two previous works provide proofs of concept, our study further investigates and evaluates different analog assimilation strategies and their detailed

implementation. Our contributions are threefold. First, we present and examine various analog forecasting strategies, including locally linear ones that were not considered in previous works, and evaluate their performance for analog data assimilation. Second, in addition to the ensemble Kalman algorithms, we propose and examine a novel implementation of the analog forecasting combined with a particle filter. Finally, in the online supplemental material, we provide a unified computational framework, through both a Matlab Toolbox and a Python Library, to pave the way for practical use and future research (<https://github.com/ptandeo/AnDA>).

The work is organized as follows. In section 2, we briefly present the general concepts of data assimilation and introduce the key ideas of analog data assimilation. Different analog forecasting strategies are introduced in section 3. Section 4 describes the different components of the proposed analog data assimilation framework and the associated algorithms. Numerical experiments for two classical chaotic dynamical systems are reported in section 5. Section 6 further discusses our work, highlights our key contributions, and proposes possible directions for future work.

2. General context

a. Model-driven data assimilation

Classically, data assimilation is based on the following discrete state space (Bocquet et al. 2010):

$$\mathbf{x}(t) = \mathcal{M}[\mathbf{x}(t-1), \boldsymbol{\eta}(t)], \quad (1)$$

$$\mathbf{y}(t) = \mathcal{H}[\mathbf{x}(t)] + \varepsilon(t), \quad (2)$$

where time $t \in \{0, \dots, T\}$ refers to the times in which observations are available. For the sake of simplicity we assume observations are at regular time steps.

In (1), \mathcal{M} characterizes the dynamical model of the true state $\mathbf{x}(t)$, while $\boldsymbol{\eta}(t)$ is a random perturbation added to represent model uncertainty. The observation equation (2) describes the relationship between the observation $\mathbf{y}(t)$ and $\mathbf{x}(t)$. Observation error is considered through the random noise $\varepsilon(t)$. Here, for the sake of simplicity, we consider an additive Gaussian noise ε with covariance \mathbf{R} in (2) and the observation operator $\mathcal{H} = \mathbf{H}$ is assumed linear.

Data assimilation aims to reconstruct the state sequence $\{\mathbf{x}(t)\}$ from a series of observations $\{\mathbf{y}(t)\}$. Two types of data assimilation schemes are extensively studied in the literature: variational and stochastic. Variational data assimilation proceeds by minimizing a cost function based on a continuous formulation of (1) and (2) (see Lorenc et al. 2000), while stochastic data assimilation

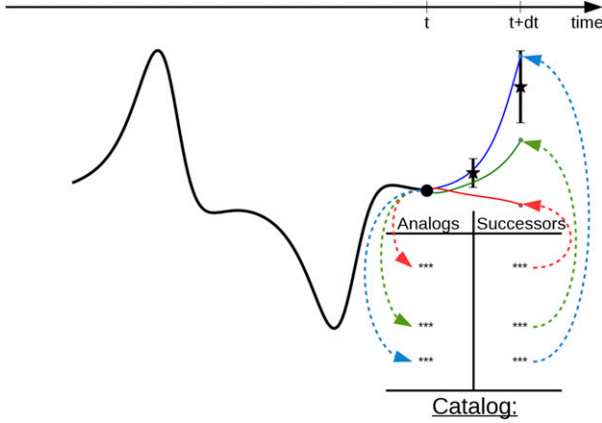


FIG. 1. The evolution in time of one particle or member. The catalog implicitly represents the dynamics of the system from exemplars of historical datasets. The observations are shown by black asterisks, and their variance is shown by the corresponding error bar.

schemes rely on the sampling and/or maximization of the posterior likelihood of the state sequence given the observation series (see Kalnay 2003). These classical data assimilation schemes are regarded as “model driven,” in the sense that they combine observations with forecasts provided by a numerical model \mathcal{M} .

b. Data-driven data assimilation

The proposed assimilation framework relies on a similar state-space formulation. The key feature is to substitute the explicit dynamical model \mathcal{M} in (1) by a “data driven” dynamical model involving an analog forecasting operator, denoted by \mathcal{A} , namely,

$$\mathbf{x}(t) = \mathcal{A}[\mathbf{x}(t-1), \boldsymbol{\eta}(t)]. \quad (3)$$

Henceforth, this state-space model will be referred to as AnDA. A sequential and stochastic data assimilation scheme including filtering and smoothing, is used involving different Monte Carlo realizations of the state at each assimilation time. We sketch the proposed AnDA methodology for one realization in Fig. 1.

The analog forecasting operator \mathcal{A} requires the existence of a representative dataset of exemplars of the considered dynamics. This dataset is referred to as the *catalog* and denoted by \mathcal{C} . The reference catalog is formed by pairs of consecutive state vectors, separated by the same time lag. The second component of each pair is referred to as the successor of the first component hereafter. The catalog may be issued from observational data as well as from numerical simulations. In the last case, one can have a catalog issued from numerical simulations (based on physical equations), and wants to perform data assimilation without running the model

again. This is for instance useful for operational prediction centers that do not have the computational resources to integrate a forecast model, but do have access to a large database of numerical simulations or analysis data of a large prediction center. In this respect, we discuss also the situation where the catalog comprises noisy versions of the true states (section 5d).

Given a catalog \mathcal{C} , the analog forecasting operator \mathcal{A} is stated as an exemplar-based statistical emulator of the state \mathbf{x} from time t to time $t + dt$. For any state $\mathbf{x}(t)$, we emulate the following state at time $t + dt$ based on its nearest neighbors in catalog \mathcal{C} . Given the analog forecasting operator, we present associated stochastic assimilation schemes, namely the *analog ensemble Kalman filter/smoothen* (Tandeo et al. 2015a) and the *analog particle filter*.

3. Analog forecasting strategies

a. Analog forecasting operator

Let us consider a kernel function, denoted by g , in the state space (Schölkopf and Smola 2001). Among the classical choices for kernels, we consider here a radial basis function (also referred to as a Gaussian kernel):

$$g(u, v) = \exp(-\lambda \|u - v\|^2), \quad (4)$$

where λ is a scale parameter, (u, v) are variables in the state space \mathcal{X} , and $\|\cdot\|$ is the Euclidean distance or another appropriate distance function. Note that the proposed analog forecasting operator may be applied to other kernels or subspace reduction methods to efficiently retrieve relevant analog situations. This is discussed in section 6.

Given the considered kernel, the analog forecasting operator \mathcal{A} is defined as follows: for a given state $\mathbf{x}(t)$, we denote by $a_k[\mathbf{x}(t)]$ its k th nearest neighbor (or analog situation) in the reference catalog of exemplars \mathcal{C} , and by $s_k[\mathbf{x}(t)]$ the known successor of state $a_k[\mathbf{x}(t)]$. Hereinafter, we refer by K to the number of nearest neighbors (analog), and by cov_w the weighted covariance. The normalized kernel weight for every pair $\{a_k[\mathbf{x}(t)], s_k[\mathbf{x}(t)]\}$ is given by

$$\omega_k[\mathbf{x}(t)] = \frac{g\{\mathbf{x}(t), a_k[\mathbf{x}(t)]\}}{\sum_{k=1}^K g\{\mathbf{x}(t), a_k[\mathbf{x}(t)]\}}. \quad (5)$$

Several ideas can be explored to define the analog forecasting operator \mathcal{A} . The natural first option consists in deriving the forecast using the weighted mean of the K successors. This approach, that we call here the *locally constant* operator, was considered in many analog forecasting related works (McDermott and Wikle 2016;

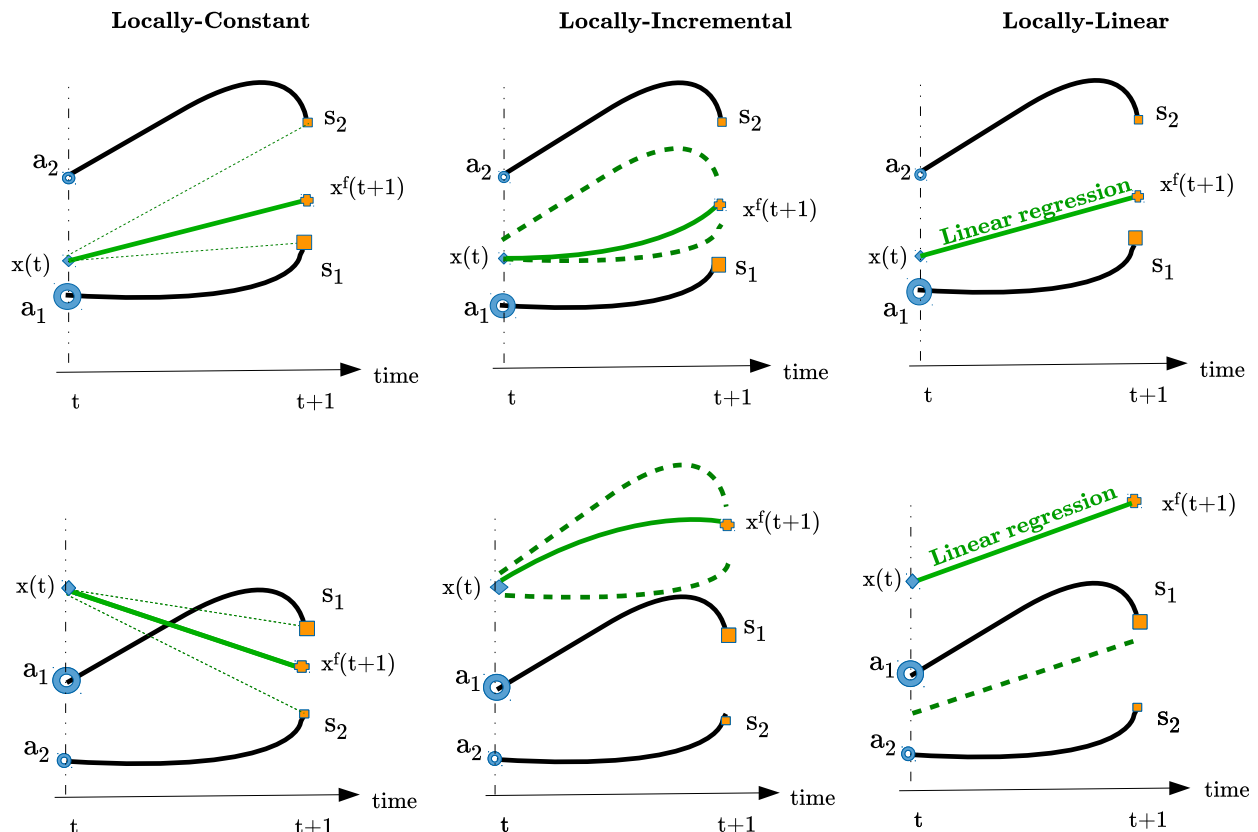


FIG. 2. A simplified illustration of the considered analog forecasting strategies in the case of two analogs (nearest neighbors). Two situations for the state $x(t)$ are shown: (top) a situation where $x(t)$ lies in the convex hull spanned by catalog exemplars and (bottom) a situation where $x(t)$ lies farther from its analogs. The second situation is expected to occur more often for high-dimensional space as well as for states, which are less likely. The latter may model extreme events or outliers.

Zhao and Giannakis 2014; Hamilton et al. 2016), and is also known in statistics as Nadaraya–Watson kernel regression. One can also use as analog forecasting operator the weighted mean of the anomalies between the K analogs and their successors and adding it to the state to derive the forecast. The operator, referred to as *locally incremental*, is seen as more physically sound and relates more closely to a finite-difference approximation of the underlying differential equations. Finally, we introduce in this work a new analog forecasting operator that makes use of local linear regression techniques based on weighted least squares estimates. This operator that we call the *locally linear* operator is known to make an efficient use of small datasets and to reduce biases (Cleveland 1979). Note that the locally constant and locally incremental operators are two special cases of the locally linear operator.

Figure 2 shows an illustration of the three analog forecasting operators used in this work. Hereafter, we denote the forecasted state as $\mathbf{x}^f(t + dt)$. The three analog forecasting operators are defined as follows for two

sampling schemes: a Gaussian sampling and a multinomial one. Hereinafter, $\delta_Z(\cdot)$ denotes a delta function centered on Z .

- Locally constant analog operator: for the Gaussian case, the forecasted state is sampled from a Gaussian distribution whose mean m_{LC} and covariance Σ_{LC} are the weighted mean and the weighted covariance estimated from the K successors and their weights:

$$\mathbf{x}^f(t + dt) \sim \mathcal{N}(m_{LC}, \Sigma_{LC}), \quad (6)$$

where $m_{LC} = \sum_{k=1}^K \omega_k [\mathbf{x}(t)] s_k[\mathbf{x}(t)]$ and $\Sigma_{LC} = \text{cov}_{\omega}(s_k[\mathbf{x}(t)]_{k \in [1, K]})$. While in the multinomial case, the forecasted state is drawn from the multinomial discrete distribution that samples the successor $s_k[\mathbf{x}(t)]$ with a probability of ω_k :

$$\mathbf{x}^f(t + dt) \sim \sum_{k=1}^K \omega_k [\mathbf{x}(t)] \delta_{s_k[\mathbf{x}(t)]}(\cdot). \quad (7)$$

- Locally incremental analog operator: instead of considering a weighted mean of the K successors as

in the locally constant operator, we consider the value of the current state plus a weighted mean of the K increments τ_k , that is, the differences between analogs and successors $\tau_k[\mathbf{x}(t)] = s_k[\mathbf{x}(t)] - a_k[\mathbf{x}(t)]$. The Gaussian sampling is given by

$$\mathbf{x}^f(t + dt) \sim \mathcal{N}(m_{\text{LI}}, \Sigma_{\text{LI}}), \quad (8)$$

where $m_{\text{LI}} = \mathbf{x}(t) + \sum_{k=1}^K \omega_k[\mathbf{x}(t)] \tau_k[\mathbf{x}(t)] = \sum_{k=1}^K \omega_k[\mathbf{x}(t)] \{\mathbf{x}(t) + \tau_k[\mathbf{x}(t)]\}$ and $\Sigma_{\text{LI}} = \text{cov}_\omega(\{\mathbf{x}(t) + \tau_k[\mathbf{x}(t)]\}_{k \in [1, K]})$ and the multinomial sampling resorts to

$$\mathbf{x}^f(t + dt) \sim \sum_{k=1}^K \omega_k[\mathbf{x}(t)] \delta_{\mathbf{x}(t) + \tau_k[\mathbf{x}(t)]}(\cdot). \quad (9)$$

- **Locally linear analog operator:** we fit a multivariate linear regression between the K analogs of the current state and their corresponding successors using weighted least squares estimates (see [Cleveland 1979](#)). The regression gives slope $\alpha[\mathbf{x}(t)]$ and intercept $\beta[\mathbf{x}(t)]$ parameters, and residuals $\xi_k[\mathbf{x}(t)] = s_k[\mathbf{x}(t)] - (\alpha[\mathbf{x}(t)]a_k[\mathbf{x}(t)] + \beta[\mathbf{x}(t)])$. The Gaussian sampling comes to

$$\mathbf{x}^f(t + dt) \sim \mathcal{N}(m_{\text{LL}}, \Sigma_{\text{LL}}), \quad (10)$$

with $m_{\text{LL}} = \alpha[\mathbf{x}(t)]\mathbf{x}(t) + \beta[\mathbf{x}(t)]$ and $\Sigma_{\text{LL}} = \text{cov}(\xi_k[\mathbf{x}(t)]_{k \in [1, K]})$, while the multinomial sampling is given by

$$\mathbf{x}^f(t + dt) \sim \sum_{k=1}^K \omega_k[\mathbf{x}(t)] \delta_{m_{\text{LL}} + \xi_k[\mathbf{x}(t)]}(\cdot). \quad (11)$$

The choice of one operator over another depends mostly on the available computational resource and the complexity of the application. Locally constant and locally increment operators are less time and memory consuming than the locally linear operator, and while they can be of comparable performance in case of a flat regression function, the locally linear is expected to better deal with curvier regression functions at the expense, however, of the requirement of a larger number of analogs to fit the regression ([Hansen 2000](#)). The locally linear and the locally incremental are more suitable for samples near or outside the boundary of the select analogs (as depicted in [Fig. 2](#)), this may be particularly relevant in geoscience applications where chaos and extreme events are of high interest.

b. Global and local analogs

The global analog strategy is the direct application of the introduced analog forecasting strategies to the entire state vector. We also introduce a local analog forecasting operator. For a given state $\mathbf{x}(t)$, the analogs $a_k[\mathbf{x}_l(t)]$ in the reference catalog, and their associated

successors $s_k[\mathbf{x}_l(t)]$ for each component l of the state $\mathbf{x}(t)$ are defined according to a component-wise local neighborhood, typically $\{\mathbf{x}_{l-\nu}(t), \dots, \mathbf{x}_l(t), \dots, \mathbf{x}_{l+\nu}(t)\}$ with ν being the width of the considered component-wise neighborhood, such that the evaluation of the kernel function and the computation of the associated normalized weights $\omega_k[\mathbf{x}_l(t)]$ only involve this local neighborhood.

The idea of using local analogs is motivated by the fact that points tends to scatter far away from each other in high dimensions, which make the search for skillful analogs nearly impossible for high-dimensional state space. For instance, [Van den Dool \(1994\)](#) has shown that finding a relevant analog at synoptic scale over the Northern Hemisphere for atmospheric data would require 10^{30} years of data to match the observational errors at that time. Conversely, analog forecasting schemes may only apply to systems or subsystems associated with low-dimensional embedding. Following this analysis, the analog forecasting of the global state is split as a series of local and low-dimensional analog forecasting operations. Note that such local analogs also reduce possible spurious correlations.

4. Analog data assimilation

The analog data assimilation is stated as a sequential and stochastic assimilation scheme, using Monte Carlo methods. It amounts to estimating the so-called filtering and smoothing posterior likelihoods, respectively, $p[\mathbf{x}(t) | \mathbf{y}(1), \dots, \mathbf{y}(t)]$ the distribution of the current state knowing past and current observations and $p[\mathbf{x}(t) | \mathbf{y}(1), \dots, \mathbf{y}(T)]$ the distribution of the current state knowing past, current, and future observations. We investigate both ensemble Kalman filter/smoothing and particle filter.

a. Analog ensemble Kalman filter and smoother (AnEnKF/AnEnKS)

Ensemble Kalman filters (EnKF) and smoothers (EnKS) ([Burgers et al. 1998](#); [Evensen 2007](#)) are particularly popular in geoscience as they provide flexible assimilation strategies for high-dimensional states. They rely on the assumption that the filtering and smoothing posteriors are multivariate Gaussian distributions, such that the following forward and backward recursions are derived. The next two paragraphs present the AnEnKF and AnEnKS equations, which are equivalent to those of the EnKF and EnKS described in [Tandeo et al. \(2015b\)](#), except for the update step where we use the analog forecasting operator.

The forward recursions of the AnEnKF correspond to the stochastic EnKF algorithm proposed by [Burgers](#)

et al. (1998) in which observations are treated as random variables. The AnEnKF algorithm starts at time $t = 1$ by generating the vectors $\mathbf{x}_i^f(1) \forall i \in \{1, \dots, N\}$ using a multivariate Gaussian random generator with mean vector \mathbf{x}^b and covariance matrix \mathbf{B} . The index i of the state vector corresponds to the i th realization of the Monte Carlo procedure (called member or particle). Then the update step proceeds from $t = 2$ to $t = T$ by applying the analog forecasting operator to each member of the ensemble following (3) to generate $\mathbf{x}_i^f(t)$. The forecast state is represented by the sample mean $\bar{\mathbf{x}}^f(t)$ and the sample covariance $\mathbf{P}^f(t)$. In the analysis step, following (2), N samples of $\mathbf{y}_i^f(t)$ are generated from a multivariate Gaussian random generator with mean $\mathbf{H}\bar{\mathbf{x}}_i^f(t)$ and covariance \mathbf{R} . The observations are then used to update the N members of the ensemble as $\mathbf{x}_i^a(t) = \mathbf{x}_i^f(t) + \mathbf{K}^a(t)[\mathbf{y}(t) - \bar{\mathbf{y}}_i^f(t)]$, where $\mathbf{K}^a(t) = \mathbf{P}^f(t)\mathbf{H}'[\mathbf{H}\mathbf{P}^f(t)\mathbf{H}' + \mathbf{R}]^{-1}$ is the Kalman filter gain. The filtering posterior distribution is then represented by the sample mean $\bar{\mathbf{x}}^a(t)$ and the sample covariance $\mathbf{P}^a(t)$.

The analog ensemble Kalman smoother combines the analog forecasting operator and the classical Kalman smoother, here, Rauch–Tung–Striebel smoother [see Cosme et al. (2012) for more details]. Given the forward recursion, the backward recursion starts from time $t = T$ with filtered state, $\forall i \in \{1, \dots, N\}$, such as $\mathbf{x}_i^s(T) = \mathbf{x}_i^a(T)$ and $\mathbf{P}^s(T) = \mathbf{P}^a(T)$. Then, we proceed backward from $t = T - 1$ to $t = 1$. At each time t , we compute $\mathbf{x}_i^s(t) = \mathbf{x}_i^a(t) + \mathbf{K}^s(t)[\mathbf{x}_i^s(t+1) - \bar{\mathbf{x}}_i^f(t+1)]$, where $\mathbf{K}^s(t) = \mathbf{P}^a(t)\mathcal{M}'[\mathbf{P}^f(t+1)]^{-1}$ is the Kalman smoother gain. Note that we empirically estimate $\mathbf{P}^a(t)\mathcal{M}'$ as the sample covariance matrix of the ensemble members as in Pham (2001) or Tandeo et al. (2015b) in the case of a nonlinear operator \mathcal{M} . The smoothing posterior distribution is represented by the sample mean $\bar{\mathbf{x}}^s(t)$ and the sample covariance $\mathbf{P}^s(t)$.

We note that the following way of extending EnKF and EnKS to become analog-based algorithms can be applied in the same way to other flavors of EnKF such as the square root ensemble Kalman filter (EnSRF). We chose stochastic ensemble-based Kalman filters and smoothers as an illustration in this work, even if they are not the first choice in practice for atmospheric and oceanic applications because of issues related to perturbing observations with noise (Bowler et al. 2013). Besides, the work of Hoteit et al. (2015), where the authors address this issue, suggests that the stochastic EnKF is worth a reevaluation for oceanic and atmospheric applications.

b. Analog particle filter (AnPF)

We also implement particle filtering techniques for the proposed analog data assimilation strategy. Contrary to

the Kalman filters, particle filters do not assume a Gaussian distribution of the state. The key principle is to estimate the posteriors of the state from a set of particles (equivalent to members in the terminology used for ensemble Kalman filters).

Given an analog forecasting operator, we consider an application of the classical particle filter (Van Leeuwen 2009). From an initialization similar to the EnKF, the particle filter applies a forward recursion from time $t = 1$ to $t = T$ as follows. At time step t , we first apply the considered analog forecasting operator \mathcal{A} to forecast $\mathbf{x}_i^f(t) \forall i \in \{1, \dots, N\}$ from previous filtered particles $\mathbf{x}_i^a(t-1)$. Then, following (2), we compute particle weights $\pi_i(t)$ as

$$\pi_i(t) \propto \phi[\mathbf{y}(t) - \mathbf{H}\mathbf{x}_i^f(t); \mathbf{R}], \quad (12)$$

where $\phi(\cdot; \mathbf{R})$ is a centered multivariate Gaussian distribution with covariance \mathbf{R} . Weights $\pi_i(t)$ are normalized to total one. We then proceed to a systematic resampling from the multinomial distribution defined by the particles $\{\mathbf{x}_i^f(t)\}$ and their corresponding weights $\{\pi_i(t)\}$. The analyzed state $\bar{\mathbf{x}}^a(t)$ is typically computed as the sample mean

$$\bar{\mathbf{x}}^a(t) = \frac{1}{N} \sum_{i=1}^N \pi_i(t) \mathbf{x}_i^f(t), \quad (13)$$

but one may also consider the posterior mode as the filtered state.

In theory, particle smoothers may also be considered. Different strategies have been proposed in the past but they showed numerical instabilities in preliminary experiments with the considered analog forecasting operator. We do not further detail the considered implementation but discuss these aspects in section 6.

5. Numerical experiments

To evaluate the relevance and performance of the proposed analog data assimilation, we consider numerical experiments on dynamical systems extensively used in the literature on data assimilation: Lorenz-63 and Lorenz-96 models. The experiments for evaluating the effect of the size of the catalog, the impact of noisy catalogs, and catalogs with parametric model error are conducted using the Lorenz-63 model. To evaluate the global and local analog forecasting operators we use the Lorenz-96 model, an extended dynamical nonlinear system with 40 variables.

a. Chaotic models

We first consider the chaotic Lorenz-63 system. From a methodological point of view, it is particularly

interesting because of its nonlinear chaotic behavior and low dimension. Several works have used this system (e.g., Miller et al. 1994; Anderson and Anderson 1999; Pham 2001; Chin et al. 2007; Hoteit et al. 2008 or Van Leeuwen 2010). The Lorenz-63 model is defined by

$$\begin{aligned}\frac{dx_1(t)}{dt} &= \sigma[x_2(t) - x_1(t)], \\ \frac{dx_2(t)}{dt} &= x_1(t)[\gamma - x_3(t)] - x_2(t), \\ \frac{dx_3(t)}{dt} &= x_1(t)x_2(t) - \beta x_3(t),\end{aligned}\quad (14)$$

and behaves chaotically for certain sets of parameters, such as ($\sigma = 10$, $\gamma = 28$, $\beta = 8/3$). Here, we use the explicit (4, 5) Runge–Kutta integrating method (cf. Dormand and Prince (1980)) with time step $dt = 0.01$ (nondimensional units). As in Van Leeuwen (2010) only the first variable of the Lorenz-63 system (x_1) is observed every 8 integration time steps (i.e., with $dt = 0.08$). Considering the analogy between the Lorenz-63 and atmospheric time scales, it is equivalent to a 6-h time step in the atmosphere.

The Lorenz-96 model is another chaotic model largely used for evaluating data assimilation techniques in geophysics (Anderson 2001; Whitaker and Hamill 2002; Ott et al. 2004; Anderson 2007, 2012; Hoteit et al. 2012). It is defined by

$$\frac{dx_j(t)}{dt} = [-x_{j-2}(t) + x_{j+1}(t)]x_{j-1}(t) - x_j(t) + F, \quad (15)$$

where $j = 1, \dots, n$ and the boundaries are cyclic [i.e., $x_{-1}(t) = x_{n-1}(t)$, $x_0(t) = x_n(t)$, and $x_{n+1}(t) = x_1(t)$]. The three right-hand side terms in (15) simulate an advection, a diffusion, and a forcing term, respectively. As in Lorenz (1996), we choose $n = 40$ and external forcing of $F = 8$ for which the model behaves chaotically. Equation (15) is solved using the Runge–Kutta fourth-order scheme with integration time step $dt = 0.05$, corresponding to a time step of 6 h in the atmosphere. Observations are taken from half of the state vector (20 observed components randomly selected) every 4 time steps (i.e., $dt = 0.20$).

b. Experimental details

The considered experimental setting is as follows. To avoid divergence of the filtering methods, we use $N = 100$ members/particles for the Lorenz-63 and $N = 1000$ members/particles for the Lorenz-96 for both model-driven and data-driven strategies. We use the same covariance matrix \mathbf{R} with a noise observation variance set to 2. To avoid any spinup effect, the initial state conditions is chosen as the ground truth mean and a covariance matrix

\mathbf{B} with noise variance 0.1. To compare the technique performances, we use the root-mean-square error (RMSE) on all the components of the state vector and for all assimilation times. As training dataset for the catalog and test dataset for RMSE computation, we use 10^3 and 100 Lorenz times, respectively.

The analog forecasting operator involves two free parameters, namely, K the number of nearest neighbors and λ the scale parameter of the Gaussian kernel in (4). Two strategies can be considered for K : either a predefined number of nearest neighbors, or a predefined threshold on distance d_{th} to select the analogs that are closer than d_{th} . For the sake of simplicity, we consider in this work the first alternative and set K to 50. Besides, we use for λ the following adaptive rule: $\lambda[x(t)] = 1/md[x(t)]$, where $md[x(t)]$ is the median distance between the current state $x(t)$ and its K analogs. Note that a cross-validation procedure could be used to optimize the choice of K and λ . All analog forecasting operators are fitted for forecasting time horizon corresponding to the time step of the numerical simulations (i.e., $dt = 0.01$ for Lorenz-63 experiments and $dt = 0.05$ for Lorenz-96 experiments). Numerical experiments (not reported here) show that this parameterization provides on average the best forecasting performance with respect to the forecasting time horizon.

c. Experiments with Lorenz-96 model

1) EXPERIMENT 1

The first numerical experiment consisted only in the application of analog forecasting (without assimilation) from a catalog. We build a database using Lorenz-96 equations, then we split the samples randomly to 2/3 for training the analog forecasting operators and 1/3 for test. Finally, we compare the RMSE w.r.t. ground truth data as a function of Lorenz-96 forecast time. For local analogs, we consider $\nu = 2$ the width of the considered component-wise neighborhood. Figure 3 shows the results of this experiment using the three choices for the analog forecasting operator \mathcal{A} . The locally linear approach outperforms the two other approaches confirming that its forecasts are with lower bias compared to the other approaches. However, it also involves more parameters, which increases the variance of the forecasts. This bias-variance trade-off supports the greater generalization capabilities of the locally linear operator, when the dynamics can well be approximated locally by a linear operator.

Figure 3 also compares local and global analog strategies. When using locally constant operator, local analogs are always better than global analogs. Searching for nearest neighbors on 40-dimensional vectors results

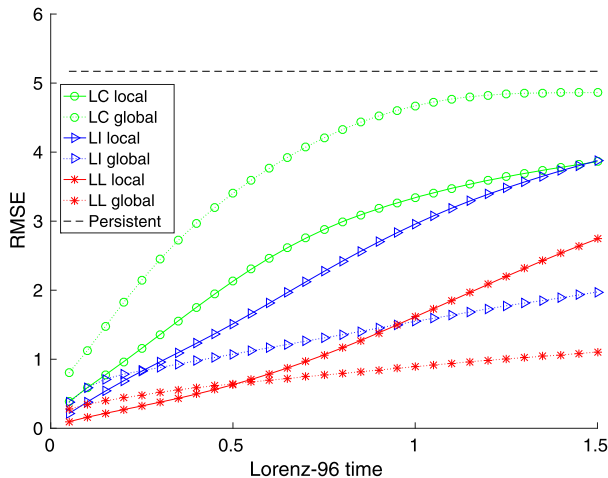


FIG. 3. Results of the analog forecasting performance as a function of the horizon. Different analog forecasting methods are plotted: locally constant (green), locally incremental (blue), and locally linear (red) analog operators with local (straight line) and global (dashed line) analog strategies. The black dashed line corresponds to a persistent prediction over time.

most likely in irrelevant analogs. This affects heavily the locally constant operator more than the two other operators, since it computes a weighted mean of their associated successors. The locally constant operator also limits novelty creation in the dynamics by always dragging the forecast near the mean of the K successors, and, according to these experiments, it seems poorly adapted to complex and highly nonlinear systems. Regarding the locally incremental and locally linear strategies, local analogs are more relevant than global ones for prediction in a near future (less than 0.5 in Lorenz-96 time for locally linear operator and less than 0.25 in Lorenz-96 time for locally incremental).

2) EXPERIMENT 2

We conducted a second experiment for evaluating the impact of analog forecasting in data assimilation using the Lorenz-96 model. We run the AnEnKS with 1000 ensemble members, only 20 variables are observed every 0.20 time steps. Figure 4 shows analog data assimilation experiments with the locally linear forecasting method using the Lorenz-96 model. Figures 4a and 4b show the true state and the observations, respectively. The reconstructed state with global analogs is shown in Fig. 4c and the one with local analogs in Fig. 4d. The local analog data assimilation experiment clearly outperforms the global analog data assimilation experiment.

3) EXPERIMENT 3

A third experiment with the Lorenz-96 system was conducted. For the local analog strategy, we further

compare the proposed AnDA algorithms, namely, AnEnKF, AnPF, and the AnEnKS using 1000 ensemble members/particles, in Table 1. Two main conclusions can be drawn: (i) EnKF algorithms outperform the particle filter and (ii) the locally linear analog forecasting operator gives the best reconstruction performance. We noticed that the AnPF suffers in the 40-dimensional Lorenz-96 system from sample impoverishment and degeneracy. Despite additional experiments with different settings, for instance, w.r.t. the number of ensemble members, the number of analogs as well as using jittering (i.e., perturbing the particles with a small noise), the AnPF still suffered from the aforementioned issues.

d. Experiments with Lorenz-63 model

1) EXPERIMENT 1

In the proposed AnDA, the size of the catalog is expected to be a critical parameter. For Lorenz-63 dynamics, we conducted different AnDA experiments varying the size of the catalog $S = \{10^1, 10^2, 10^3, 10^4\}$ in Lorenz-63 times. We consider the same setting as in Tandeo et al. (2015a) where the locally constant method with a Gaussian sampling was used for the AnEnKF, then we compare the three AnDA algorithms using 100 ensemble members/particles. As reported in Fig. 5, the RMSE decreases when the size of the catalog increases for all AnDA algorithms. Regarding filtering-only (i.e., no smoothing) AnDA algorithms, the AnPF (blue) outperforms the AnEnKF (green). This is an expected result since particle filters handle better nonlinear models and non-Gaussian probability distributions, although at a high cost in terms of computational complexity and execution time. The AnEnKS (red) clearly gives the lowest RMSE. This supports the additional benefit of the smoothing step performed by the AnEnKS. The zoom shown in the right panel of Fig. 5 highlights how the smoothing step corrects the piecewise effects resulting from the filtering step.

2) EXPERIMENT 2

Modeling uncertainty is a critical source of error in data assimilation. In this experiment we evaluate whether AnDA can manage a situation in which the catalog is composed by multiple numerical simulations, which may have parametric model error. In (14), parameters γ and β define the center of the two attractors whereas σ controls the shape of the trajectories. In Fig. 6, we depict trajectories using three sets of parameters with different values for σ : $\theta_1 = (10, 28, 8/3)$ (red), $\theta_2 = (7, 28, 8/3)$ (blue), and $\theta_3 = (13, 28, 8/3)$ (green). We generate three catalogs with Lorenz-63 trajectories

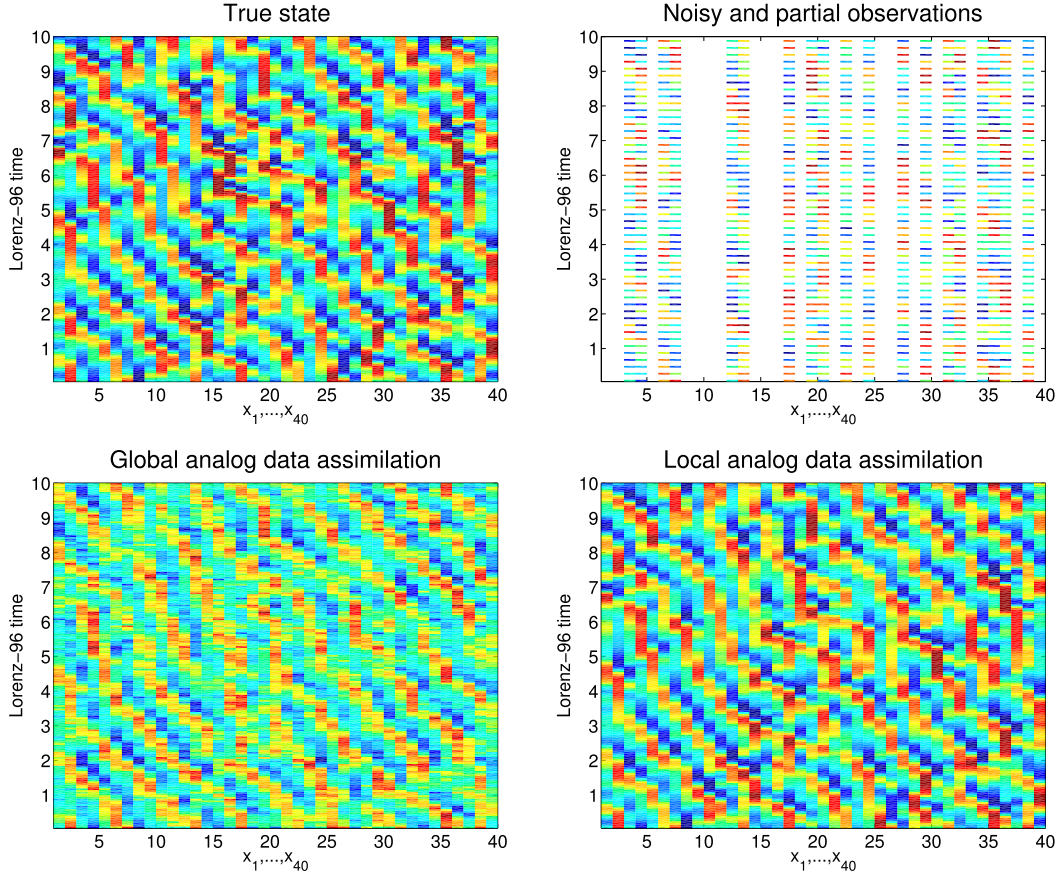


FIG. 4. Lorenz-96 trajectories obtained using analog data assimilation procedures with the locally linear forecasting strategy, when only 20 variables are observed every 0.20 time steps. (top left) True simulation of the model with 40 variables, (top right) noisy and partial observations, (bottom left) reconstructed state trajectories via the AnEnKS with global analogs, and (bottom right) reconstructed state trajectories via the AnEnKS with local analogs [taking into account the 5 ($\nu = 2$) nearest state components]. Only 10 Lorenz-96 cycles are shown for better visibility.

for these three set of parameters, with 10^3 Lorenz time steps each. Merging these three catalogs into a global catalog, we apply the proposed AnDA using as observations the true integration resulting from Lorenz-63 model with θ_1 parameter values. As a by-product of the analog strategy, we can infer the underlying model parameterization from the observed partial observations. The reported experiments (Fig. 6) apply the AnPF procedure with the locally constant analog method and a multinomial sampling scheme using 100 particles. Such a choice was motivated by the desire of keeping track of the particles and their source catalog, which is harder to achieve with the other AnDA algorithms, since the particles would be elements from the catalog and the AnPF assigns a weight to each particle. This make it easier to select at each time the particle with the biggest weight and to know from which catalog it came from.

At every assimilation time step, we determine which parameterization most ensemble members come from,

and then calculate the proportion of the presence of each parameterization. As expected, the true parameterization (red, parameterization θ_1) is more represented. The proportions for θ_1 , θ_2 , and θ_3 are around,

TABLE 1. RMSE of the reconstruction of Lorenz-96 state evolution using different forecasting strategies and data assimilation techniques. The catalog size corresponds to 10^3 Lorenz-96 times (equivalent to 13 yr) and the number of members/particles is $N = 1000$.

Method	Locally constant	Locally incremental	Locally linear
Gaussian			
AnEnKF	1.826	1.785	1.403
AnPF	3.174	4.224	4.4616
AnEnKS	1.320	1.287	0.970
Multinomial			
AnEnKF	1.814	1.774	1.413
AnPF	2.989	4.412	4.729
AnEnKS	1.313	1.288	1.093

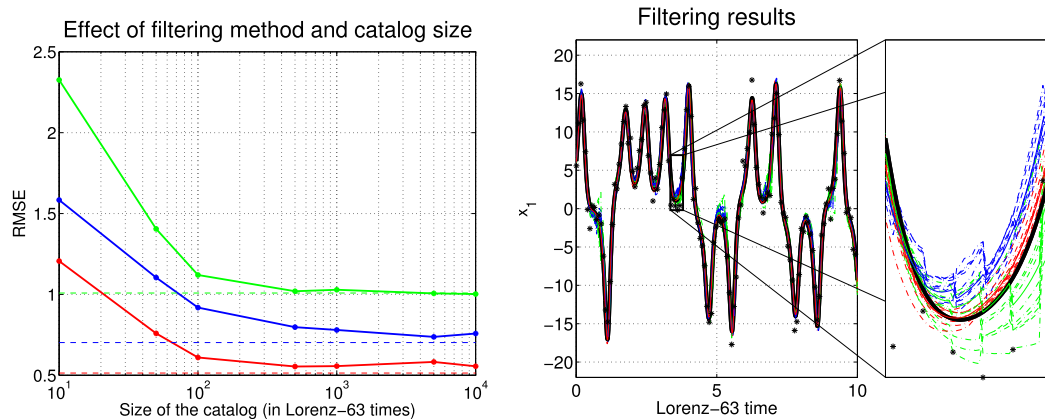


FIG. 5. Reconstruction of Lorenz-63 trajectories for different catalog sizes in the analog data assimilation procedures, when only the first component of the state is observed every 0.08 time steps. (left) RMSE as a function of the size of the catalog for different analog data assimilation strategies: AnEnKF (green), AnPF (blue), and AnEnKS (red). For benchmarking purposes, data assimilation results with true Lorenz-63 equations are given in straight lines. (right) Time series of the first component of the true state (black solid line), associated noisy observations (black asterisks), mean reconstructed series (solid lines), and 10 analyzed members/particles (dashed lines) with analog data assimilation strategies, namely AnEnKF (green), AnPF (blue), and AnEnKS (red), using a catalog of 10^3 Lorenz-63 times (equivalent to 8 yr).

60%, 16%, and 24%, respectively, proving the ability of the methodology to detect the source of the noisy and partial observation (here, only coming from θ_1). To analyze the results more thoroughly, we calculate the RMSE of the reconstruction using (i) the three catalogs as shown before, (ii) only the good catalog, and (iii) only the two “bad” catalogs. The RMSEs are (i) 1.287, (ii) 1.207, and (iii) 1.424, respectively. These results show that having other catalogs with

different parameterization degrade the RMSE but the filter is still performing well. This experiment gives insights on the problem of the assimilation of variables that may switch between different dynamical modes. Analog data assimilation can deal with this problem in a simpler manner than classical data assimilation, through the concatenation of the catalogs issued from different parameterizations into a single catalog.

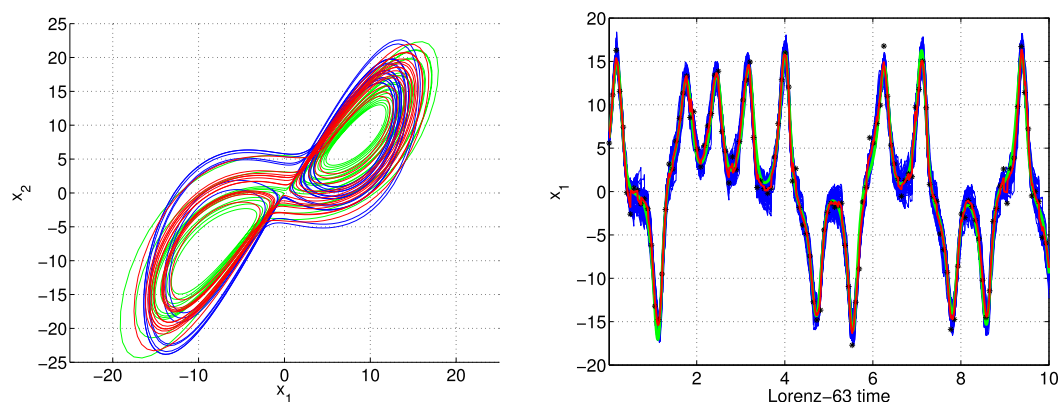


FIG. 6. Identification of Lorenz-63 model parameterizations using a multiparameterization catalog in the analog data assimilation, when only the first component of the state is observed every 0.08 time step. (left) Examples of Lorenz-63 trajectories generated with three different parameterizations: $\theta_1 = (10, 28, 8/3)$ (red), $\theta_2 = (7, 28, 8/3)$ (blue), and $\theta_3 = (13, 28, 8/3)$ (green). (right) Result of the AnPF on the first Lorenz-63 variable using the three catalogs associated with parameterizations $\{\theta_i\}_{1,2,3}$ for 3×10^3 Lorenz-63 times (equivalent to 3×8 yr) when only observations from parameterization $\theta_1 = (10, 28, 8/3)$ are provided. The figure shows the AnPF particles trajectories (blue), the AnPF result (red), and the true trajectory (green).

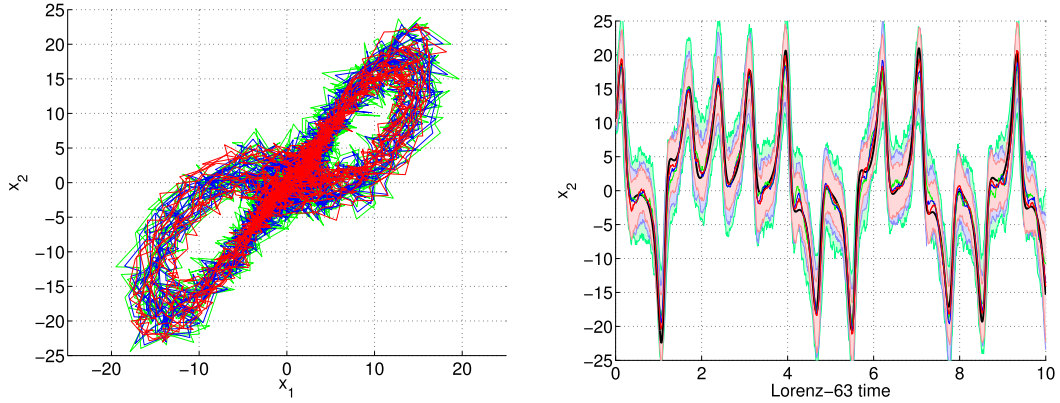


FIG. 7. Results of the reconstruction of Lorenz-63 trajectories from noisy catalogs: (left) examples of noisy Lorenz-63 trajectories for different noise levels: $\psi_1^2 = 0.5$ (red), $\psi_2^2 = 1$ (blue), and $\psi_3^2 = 2$ (green). (right) Results of the AnEnKS using noisy catalogs corresponding to 10^3 Lorenz-63 times (equivalent to 8 yr) when only observations with variance $R = 2$ are provided. We also plot the 95% confidence interval computed from the smoothing covariances.

3) EXPERIMENT 3

Whereas previous experiments consider catalogs produced from noise-free trajectories, here we evaluate the sensitivity of the AnDA procedures when the catalog may involve noisy trajectories of the considered system. Acquisition systems typically involve such noise patterns, which may relate for instance to both environmental constraints and measurement uncertainties. We simulate noisy catalogs for Lorenz-63 dynamics as follows: we artificially degrade the transition between consecutive states with a Gaussian additive noise. We performed experiments with different noise variances $\psi^2 = \{0.5, 1, 2\}$ to evaluate the sensitivity of AnDA procedures with respect to the signal-to-noise ratio. As illustrated in Fig. 7, the trajectories of these experiments are extremely noisy. Table 2 reports the RMSE of the different AnDA algorithms with the locally linear analog forecasting operator and 100 ensemble members/particles. As expected, the RMSE increases with the variance of the additive noise. The AnEnKS clearly outperforms the other AnDA algorithms, which highlights its greater robustness. Figure 7 further illustrates that the AnEnKS is able to correctly track the true state of the system, even for highly degraded catalogs ($\psi^2 = 2$, green curve). For a high signal-to-noise ratio (i.e., low perturbations) ($\psi^2 = 0.5$, red curve), reconstructed trajectories are very close to the ones obtained with a noise-free catalog.

6. Conclusions and perspectives

The present paper demonstrates the potential of data-driven schemes for data assimilation. We propose and evaluate efficient yet simple data-driven forecasting

strategies that can be coupled with classical stochastic filters (viz., the ensemble Kalman filter/smoothen and the particle filter). We set a unified framework that we call the analog data assimilation (AnDA). The key features of the AnDA are twofold: (i) it relies on a data-driven representation of the state dynamics, and (ii) it does not require online evaluations of dynamical models based on physical equations. The relevance of the AnDA is tangible when the dynamical system of interest demands tremendous and time-consuming physical modeling efforts and/or uncertainties are difficult to assess. In cases when large observational or model-simulated datasets of the considered system are available, AnDA can both support or compete with classical data assimilation schemes. As a proof concept, we demonstrate the relevance of the proposed methodology to retrieve the chaotic behavior of the Lorenz-63 and Lorenz-96 models. We performed numerical experiments to evaluate critical aspects of the method, especially the relevant combinations of analog forecasting strategies and of stochastic filters as well as the exploitation of noisy and noise-free catalogs.

TABLE 2. RMSE of the reconstruction of Lorenz-63 trajectories from noisy catalogs: we vary the variance of an additive Gaussian noise in the creation of the catalogs and apply analog data assimilation procedures with the locally linear operator with a catalog size of 10^3 Lorenz-63 times, when only the first component of the state is observed every 0.08 time step with observation noise variance $R = 2$.

Method	$\psi_1^2 = 0.5$	$\psi_2^2 = 1$	$\psi_3^2 = 2$
AnEnKF	1.926	2.136	2.681
AnPF	1.652	1.961	2.313
AnEnKS	1.233	1.561	2.142

All the reported experiments were carried out using the AnDA Python/Matlab library (<https://github.com/ptandeo/AnDA>), which includes the Lorenz-63 and Lorenz-96 systems. In the spirit of reproducible research, the user can conduct the different experiments shown in this paper.

Overall, the reported results demonstrate the relevance of the proposed analog data assimilation methods, even with highly damaged catalogs. They suggest that AnEnKS combined with locally incremental or locally linear analog forecasting leads to the best reconstruction performance, the locally incremental version being the most robust to noisy settings. Moreover, the flexibility of the analog data assimilation demonstrates the potential for the identification of hidden underlying dynamics from a series of partial observations.

The main pillar of our data-driven approach is the catalog. As such, analog data assimilation deeply relates to the quality and representativity of the catalog. In our experiments, we assumed that we were provided with large-scale catalogs of complete states of the system of interest. While catalogs built from numerical simulations fulfill this assumption, observational datasets (e.g., satellite remote sensing or in situ data) typically involve missing data, which may require specific strategies to be dealt with in the building of the catalogs. In this respect, local analogs obviously appear much more flexible than global ones, as partial observations provide relevant exemplars for the creation of catalogs for local analogs.

The application of analog data assimilation to high-dimensional systems is another future challenge. As detailed in [Van den Dool \(1994\)](#), the number of elements in a catalog shall grow exponentially with the intrinsic dimension of the state to guarantee the retrieval of analogs at a given precision. This makes unrealistic the direct application of analog strategies to state space with an intrinsic dimensionality above 10. As a consequence, global analog forecasting operators are most likely inappropriate for high-dimensional systems. By contrast, local analogs provide a means to decompose the analog forecasting of the high-dimensional state into a series of local and low-dimensional analog forecasting operations. This is regarded as the key explanation for the much better performance reported for the local analog data assimilation for Lorenz-96 dynamics using catalogs of about a million of exemplars ([Fig. 4](#)). For real-world applications to high-dimensional systems, for instance to ocean and atmosphere dynamics, the combination of such local analog strategies to multiscale decompositions ([Mallat 1989](#)) arise as a promising research direction as illustrated in [Fablet et al. \(2017\)](#). Such multiscale decompositions are expected to enhance the spatial redundancy, with a view to

building the requested catalogs of millions to hundreds of millions of exemplars (for an intrinsic dimensionality between 4 and 7, see the [appendix](#)) from observation or simulation datasets over a few decades. Another important aspect that controls the effective size of the catalog is the evolution of the system in time. The more nonlinear the dynamics, the greater the number of requested exemplars in the global catalog to learn the forecast operator and the spread of the prediction.

We believe that this study opens new research avenues for the analysis, reconstruction, and understanding of the dynamics of geophysical systems using data-driven techniques. Such techniques will benefit from the increasing availability of large-scale historical observational and/or simulated datasets. Beyond the wide range of possible applications, future research should further investigate methodological issues. First of all, our study demonstrates the relevance of the analog particle filter, but as mentioned in [section 5](#), the AnPF suffers from degeneracy and sample impoverishment. We may point out that complementary experiments with particle smoother schemes (not shown in this paper) resulted in numerical instabilities. The derivation of the analog particle smoother then remains an open question. In addition to advanced particle filters as proposed in [Van Leeuwen \(2010\)](#) and [Pitt and Shephard \(1999\)](#), one might also benefit from the straightforward applications of the analog procedure in reverse time, which is not generally possible for model-driven schemes. A second direction for future work lies in the design of the kernel used by the analog forecasting operators. Whereas we considered a Gaussian kernel, other kernels have been proposed in the literature; for example, using Procrustes distance instead of the Euclidean distance ([McDermott and Wikle 2016](#)) or different weighing strategies ([Delle Monache et al. 2011](#)). The explicit derivation of the mapping associated with a kernel as considered in [Zhao and Giannakis \(2014\)](#) may also be a promising alternative to state the analog data assimilation in a kernel-derived lower-dimensional space. The theoretical characterization of the asymptotic behavior of analog data assimilation schemes is also an interesting avenue of research. Similarly to the theoretical analysis of ensemble Kalman filters and particle filters ([Le Gland et al. 2009](#)), the derivation of convergence conditions, possibly associated with reconstruction bounds, would be of key interest to bound the reconstruction performance of the proposed analog schemes with respect to their model-driven counterpart.

Acknowledgments. We thank all the researchers from various fields who provided careful and constructive comments on the original paper especially Bertrand

Chapron, Valérie Monbet, and Anne Cuzol. The authors would also like to thank Phi Viet Huynh for his valuable contribution to both the AnDA Matlab toolbox and the AnDA Python library. We are also grateful to the two anonymous reviewers, whose comments helped to improve the manuscript. We thank Geraint Jones for his English grammar corrections. This work was supported by ANR (Agence Nationale de la Recherche, Grant ANR-13-MONU-0014), Labex Cominlabs (Grant SEACS), the Brittany council, and a “Futur et Ruptures” postdoctoral grant from Institut Mines-Télécom.

APPENDIX

Operational Count of the AnDA Applied for High-Dimensional Applications

This appendix aims at giving an estimate of the operations involved when applying the AnDA for a realistic large-scale application. We discuss the computational cost of the analog forecasting, which is specific to the AnDA. The latter directly relates to the cost of the K -nearest neighbor (K-NN) step.

In case of large-scale catalogs, an exhaustive search strategy is not suitable and the use of space-partitioning data structures, the most popular ones being *K-d trees* (Bentley 1975) and *Ball trees* (Omohundro 1989), appears necessary. These structures speed up the K-NN search, at the expense of an approximate search for nearest neighbors. Let us denote by D the dimension of the system of interest. Making a choice between K-d trees or ball trees depends mostly on the dimensionality of the system. The K-d trees are known to perform well in dimensions $D < 20$, while ball trees are more suitable to dimensions higher than 20 but come with a high cost of space partitioning (Witten et al. 2016). In this appendix we focus on the use of K-d trees, which are natural candidates for local analogs with a small component-wise local neighborhood ν or using a preliminary dimensionality reduction algorithm (such as empirical orthogonal functions). A comparison between K-d trees and ball trees is out of the scope of this work.

Let N_{data} be the size of the catalog (the number of samples from where to look for analogs), and K the number of nearest neighbors to be retrieved. Let us recall that ν is the size of the local neighborhood used for the search for local analogs. Van den Dool (1994) derived a relationship between the local neighborhood size and the amount of the data needed to find an analog with a given precision. With the assumption that the components of the states follow a multivariate Gaussian distribution and have the same variance sd^2 , finding K samples that have a distance lower than ε for all

the components of the neighborhood with a probability of 95%, needs the number of data to be on average as follows:

- Global analogs:

$$N_{\text{global}} \geq K \frac{\ln(0.05)}{\ln(1 - \alpha^D)} \simeq \frac{3K}{\alpha^D}, \quad (\text{A1})$$

- Local analogs:

$$N_{\text{local}} \geq K \frac{\ln(0.05)}{\ln(1 - \alpha^{2\nu+1})} \simeq \frac{3K}{\alpha^{2\nu+1}}, \quad (\text{A2})$$

where α is the integral of the standard Gaussian probability density function from $-\varepsilon/(\sqrt{2}sd)$ to $-\varepsilon/(\sqrt{2}sd)$.

We present now the operational count for one ensemble member (or particle) involved in the forecasting, for both global and local analogs. In each case, we distinguish the computational cost of the creation of the K-d trees and the search of K nearest neighbors:

- Global analogs:
 - Creation of the K-d tree: $O[DN_{\text{global}} \log(N_{\text{global}})]$.
 - Search for K global analogs: $O[KD \log(N_{\text{global}})]$.
- Local analogs:
 - Creation of D K-d trees (for every dimension in D): $O[D(2\nu + 1)N_{\text{local}} \log(N_{\text{local}})]$.
 - Search for K local analogs of component-wise neighborhood ν : $O[DK(2\nu + 1) \log(N_{\text{local}})]$.

Note that using local analogs requires constructing a K-d tree for every dimension in D . Construction of the K-d trees can be done offline (1 “big” K-d tree for the global strategy and D “small” K-d trees for the local strategy), then the cost of these construction can be amortized over the high number of queries that needs to be answered during analog data assimilation. However, in terms of memory storage, storing a global K-d tree could be prohibitive, contrarily to small local K-d trees that can be created, used, then freed for the creation of the next K-d tree of the next dimension (if there is no sufficient memory to stock D small local K-d trees). Keep in mind that we need to have $(2\nu + 1) \ll D$ for local analogs to be of relevance.

Let us take an example using the Lorenz-96 model: $D = 40$, $\nu = 2$. Looking for $K = 50$ analogs, with an $\alpha = 0.15$ we would need $N_{\text{global}} \approx 10^{35}$, which is very prohibitive; however, we would only need $N_{\text{local}} \approx 2 \times 10^6$ samples using local analogs.

REFERENCES

- Anderson, J. L., 2001: An ensemble adjustment Kalman filter for data assimilation. *Mon. Wea. Rev.*, **129**, 2884–2903, doi:[10.1175/1520-0493\(2001\)129<2884:AEAKFF>2.0.CO;2](https://doi.org/10.1175/1520-0493(2001)129<2884:AEAKFF>2.0.CO;2).

- , 2007: Exploring the need for localization in ensemble data assimilation using a hierarchical ensemble filter. *Physica D*, **230**, 99–111, doi:[10.1016/j.physd.2006.02.011](https://doi.org/10.1016/j.physd.2006.02.011).
- , 2012: Localization and sampling error correction in ensemble Kalman filter data assimilation. *Mon. Wea. Rev.*, **140**, 2359–2371, doi:[10.1175/MWR-D-11-00013.1](https://doi.org/10.1175/MWR-D-11-00013.1).
- , and S. L. Anderson, 1999: A Monte Carlo implementation of the nonlinear filtering problem to produce ensemble assimilations and forecasts. *Mon. Wea. Rev.*, **127**, 2741–2758, doi:[10.1175/1520-0493\(1999\)127<2741:AMCIOT>2.0.CO;2](https://doi.org/10.1175/1520-0493(1999)127<2741:AMCIOT>2.0.CO;2).
- Atencia, A., and I. Zawadzki, 2015: A comparison of two techniques for generating nowcasting ensembles. Part II: Analogs selection and comparison of techniques. *Mon. Wea. Rev.*, **143**, 2890–2908, doi:[10.1175/MWR-D-14-00342.1](https://doi.org/10.1175/MWR-D-14-00342.1).
- Bentley, J. L., 1975: Multidimensional binary search trees used for associative searching. *Commun. ACM*, **18**, 509–517, doi:[10.1145/361002.361007](https://doi.org/10.1145/361002.361007).
- Bocquet, M., C. A. Pires, and L. Wu, 2010: Beyond Gaussian statistical modeling in geophysical data assimilation. *Mon. Wea. Rev.*, **138**, 2997–3023, doi:[10.1175/2010MWR3164.1](https://doi.org/10.1175/2010MWR3164.1).
- Bowler, N. E., J. Flowerdew, and S. R. Pring, 2013: Tests of different flavours of EnKF on a simple model. *Quart. J. Roy. Meteor. Soc.*, **139**, 1505–1519, doi:[10.1002/qj.2055](https://doi.org/10.1002/qj.2055).
- Burgers, G., P. Jan van Leeuwen, and G. Evensen, 1998: Analysis scheme in the ensemble Kalman filter. *Mon. Wea. Rev.*, **126**, 1719–1724, doi:[10.1175/1520-0493\(1998\)126<1719:ASITEK>2.0.CO;2](https://doi.org/10.1175/1520-0493(1998)126<1719:ASITEK>2.0.CO;2).
- Chin, T., M. Turmon, J. Jewell, and M. Ghil, 2007: An ensemble-based smoother with retrospectively updated weights for highly nonlinear systems. *Mon. Wea. Rev.*, **135**, 186–202, doi:[10.1175/MWR3353.1](https://doi.org/10.1175/MWR3353.1).
- Cleveland, W. S., 1979: Robust locally weighted regression and smoothing scatterplots. *J. Amer. Stat. Assoc.*, **74**, 829–836, doi:[10.1080/01621459.1979.10481038](https://doi.org/10.1080/01621459.1979.10481038).
- Cosme, E., J. Verron, P. Brasseur, J. Blum, and D. Auroux, 2012: Smoothing problems in a Bayesian framework and their linear Gaussian solutions. *Mon. Wea. Rev.*, **140**, 683–695, doi:[10.1175/MWR-D-10-05025.1](https://doi.org/10.1175/MWR-D-10-05025.1).
- Delle Monache, L., T. Nipen, Y. Liu, G. Roux, and R. Stull, 2011: Kalman filter and analog schemes to postprocess numerical weather predictions. *Mon. Wea. Rev.*, **139**, 3554–3570, doi:[10.1175/2011MWR3653.1](https://doi.org/10.1175/2011MWR3653.1).
- , I. Djalalova, and J. Wilczak, 2014: Analog-based postprocessing methods for air quality forecasting. *Air Pollution Modeling and Its Application XXIII*, D. Steyn and R. Mathur, Eds., Springer, 237–239, doi:[10.1007/978-3-319-04379-1_38](https://doi.org/10.1007/978-3-319-04379-1_38).
- Dormand, J. R., and P. J. Prince, 1980: A family of embedded Runge–Kutta formulae. *J. Comput. Appl. Math.*, **6**, 19–26, doi:[10.1016/0771-050X\(80\)90013-3](https://doi.org/10.1016/0771-050X(80)90013-3).
- Evensen, G., 2007: *Data Assimilation: The Ensemble Kalman Filter*. Springer-Verlag, 280 pp., doi:[10.1007/978-3-540-38301-7](https://doi.org/10.1007/978-3-540-38301-7).
- , and P. J. Van Leeuwen, 2000: An ensemble Kalman smoother for nonlinear dynamics. *Mon. Wea. Rev.*, **128**, 1852–1867, doi:[10.1175/1520-0493\(2000\)128<1852:AEKSFN>2.0.CO;2](https://doi.org/10.1175/1520-0493(2000)128<1852:AEKSFN>2.0.CO;2).
- Fablet, R., P. H. Viet, R. Lguensat, and B. Chapron, 2017: Data-driven assimilation of irregularly-sampled image time series. *IEEE Int. Conf. on Image Processing (ICIP 2017)*, Beijing, China, IEEE, WQ-PB.2.
- Hamilton, F., T. Berry, and T. Sauer, 2016: Ensemble Kalman filtering without a model. *Phys. Rev. X*, **6**, 011021, doi:[10.1103/PhysRevX.6.011021](https://doi.org/10.1103/PhysRevX.6.011021).
- Hansen, B., 2000: *Econometrics*. Department of Economics, University of Wisconsin, 427 pp., <http://www.ssc.wisc.edu/~bhansen/econometrics/Econometrics.pdf>.
- He-Guelton, L., R. Fablet, B. Chapron, and J. Tournadre, 2015: Learning-based emulation of sea surface wind fields from numerical model outputs and SAR data. *IEEE J. Sel. Top. Appl. Earth Obs. Remote Sens.*, **8**, 4742–4750, doi:[10.1109/JSTARS.2015.2496503](https://doi.org/10.1109/JSTARS.2015.2496503).
- Hong, S.-Y., and J. Dudhia, 2012: Next-generation numerical weather prediction: Bridging parameterization, explicit clouds, and large eddies. *Bull. Amer. Meteor. Soc.*, **93**, ES6–ES9, doi:[10.1175/2011BAMS3224.1](https://doi.org/10.1175/2011BAMS3224.1).
- Hoteit, I., D.-T. Pham, G. Triantafyllou, and G. Korres, 2008: A new approximate solution of the optimal nonlinear filter for data assimilation in meteorology and oceanography. *Mon. Wea. Rev.*, **136**, 317–334, doi:[10.1175/2007MWR1927.1](https://doi.org/10.1175/2007MWR1927.1).
- , X. Luo, and D.-T. Pham, 2012: Particle Kalman filtering: A nonlinear Bayesian framework for ensemble Kalman filters. *Mon. Wea. Rev.*, **140**, 528–542, doi:[10.1175/2011MWR3640.1](https://doi.org/10.1175/2011MWR3640.1).
- , D.-T. Pham, M. Gharamti, and X. Luo, 2015: Mitigating observation perturbation sampling errors in the stochastic EnKF. *Mon. Wea. Rev.*, **143**, 2918–2936, doi:[10.1175/MWR-D-14-00088.1](https://doi.org/10.1175/MWR-D-14-00088.1).
- Kalnay, E., 2003: *Atmospheric Modeling, Data Assimilation and Predictability*. Cambridge University Press, 345 pp.
- Le Gland, F., V. Monbet, and V.-D. Tran, 2009: Large sample asymptotics for the ensemble Kalman filter. Research Rep. RR-7014, INRIA, 25 pp., <https://hal.inria.fr/inria-00409060/document>.
- Lorenc, A., and Coauthors, 2000: The Met. Office global three-dimensional variational data assimilation scheme. *Quart. J. Roy. Meteor. Soc.*, **126**, 2991–3012, doi:[10.1002/qj.49712657002](https://doi.org/10.1002/qj.49712657002).
- Lorenz, E. N., 1969: Atmospheric predictability as revealed by naturally occurring analogues. *J. Atmos. Sci.*, **26**, 636–646, doi:[10.1175/1520-0469\(1969\)26<636:APARBN>2.0.CO;2](https://doi.org/10.1175/1520-0469(1969)26<636:APARBN>2.0.CO;2).
- , 1996: Predictability—A problem partly solved. *Proc. Seminar on Predictability*, Reading, United Kingdom, ECMWF, 18 pp., <https://www.ecmwf.int/sites/default/files/elibrary/1995/10829-predictability-problem-partly-solved.pdf>.
- Mallat, S. G., 1989: A theory for multiresolution signal decomposition: The wavelet representation. *IEEE Trans. Pattern Anal. Mach. Intell.*, **11**, 674–693, doi:[10.1109/34.192463](https://doi.org/10.1109/34.192463).
- McDermott, P. L., and C. K. Wikle, 2016: A model-based approach for analog spatio-temporal dynamic forecasting. *Environmetrics*, **27**, 70–82, doi:[10.1002/env.2374](https://doi.org/10.1002/env.2374).
- Miller, R. N., M. Ghil, and F. Gauthiez, 1994: Advanced data assimilation in strongly nonlinear dynamical systems. *J. Atmos. Sci.*, **51**, 1037–1056, doi:[10.1175/1520-0469\(1994\)051<1037:ADAISN>2.0.CO;2](https://doi.org/10.1175/1520-0469(1994)051<1037:ADAISN>2.0.CO;2).
- Nagarajan, B., L. Delle Monache, J. P. Hacker, D. L. Rife, K. Searight, J. C. Knivel, and T. N. Nipen, 2015: An evaluation of analog-based postprocessing methods across several variables and forecast models. *Wea. Forecasting*, **30**, 1623–1643, doi:[10.1175/WAF-D-14-00081.1](https://doi.org/10.1175/WAF-D-14-00081.1).
- Omohundro, S. M., 1989: Five balltree construction algorithms. International Computer Science Institute, Berkeley, CA, 22 pp., <http://ftp.icsi.berkeley.edu/ftp/pub/techreports/1989/tr-89-063.pdf>.
- Ott, E., and Coauthors, 2004: A local ensemble Kalman filter for atmospheric data assimilation. *Tellus*, **56A**, 415–428, doi:[10.3402/tellusa.v56i5.14462](https://doi.org/10.3402/tellusa.v56i5.14462).
- Pham, D. T., 2001: Stochastic methods for sequential data assimilation in strongly nonlinear systems. *Mon. Wea. Rev.*, **129**, 1194–1207, doi:[10.1175/1520-0493\(2001\)129<1194:SMFSDA>2.0.CO;2](https://doi.org/10.1175/1520-0493(2001)129<1194:SMFSDA>2.0.CO;2).

- Pitt, M. K., and N. Shephard, 1999: Filtering via simulation: Auxiliary particle filters. *J. Amer. Stat. Assoc.*, **94**, 590–599, doi:[10.1080/01621459.1999.10474153](https://doi.org/10.1080/01621459.1999.10474153).
- Ruiz, J. J., M. Pulido, and T. Miyoshi, 2013: Estimating model parameters with ensemble-based data assimilation: A review. *J. Meteor. Soc. Japan*, **91**, 79–99, doi:[10.2151/jmsj.2013-201](https://doi.org/10.2151/jmsj.2013-201).
- Schenk, F., and E. Zorita, 2012: Reconstruction of high resolution atmospheric fields for northern Europe using analog-upscaling. *Climate Past*, **8**, 1681–1703, doi:[10.5194/cp-8-1681-2012](https://doi.org/10.5194/cp-8-1681-2012).
- Schölkopf, B., and A. J. Smola, 2001: *Learning with Kernels: Support Vector Machines, Regularization, Optimization, and Beyond*. MIT Press, 648 pp.
- Tandeo, P., and Coauthors, 2015a: Combining analog method and ensemble data assimilation: Application to the Lorenz-63 chaotic system. *Machine Learning and Data Mining Approaches to Climate Science*, V. Lakshmanan et al., Eds., Springer, 3–12, doi:[10.1007/978-3-319-17220-0_1](https://doi.org/10.1007/978-3-319-17220-0_1).
- , M. Pulido, and F. Lott, 2015b: Offline parameter estimation using EnKF and maximum likelihood error covariance estimates: Application to a subgrid-scale orography parametrization. *Quart. J. Roy. Meteor. Soc.*, **141**, 383–395, doi:[10.1002/qj.2357](https://doi.org/10.1002/qj.2357).
- Van den Dool, H., 1994: Searching for analogues, how long must we wait? *Tellus*, **46A**, 314–324, doi:[10.3402/tellusa.v46i3.15481](https://doi.org/10.3402/tellusa.v46i3.15481).
- Van Leeuwen, P. J., 2009: Particle filtering in geophysical systems. *Mon. Wea. Rev.*, **137**, 4089–4114, doi:[10.1175/2009MWR2835.1](https://doi.org/10.1175/2009MWR2835.1).
- , 2010: Nonlinear data assimilation in geosciences: An extremely efficient particle filter. *Quart. J. Roy. Meteor. Soc.*, **136**, 1991–1999, doi:[10.1002/qj.699](https://doi.org/10.1002/qj.699).
- Whitaker, J. S., and T. M. Hamill, 2002: Ensemble data assimilation without perturbed observations. *Mon. Wea. Rev.*, **130**, 1913–1924, doi:[10.1175/1520-0493\(2002\)130<1913:EDAWPO>2.0.CO;2](https://doi.org/10.1175/1520-0493(2002)130<1913:EDAWPO>2.0.CO;2).
- Wilby, R. L., and T. Wigley, 1997: Downscaling general circulation model output: A review of methods and limitations. *Prog. Phys. Geogr.*, **21**, 530–548, doi:[10.1177/030913339702100403](https://doi.org/10.1177/030913339702100403).
- Witten, I. H., E. Frank, M. A. Hall, and C. J. Pal, 2016: *Data Mining: Practical Machine Learning Tools and Techniques*. 4th ed. Morgan Kaufmann, 654 pp.
- Yiou, P., 2014: AnaWEGE: A weather generator based on analogues of atmospheric circulation. *Geosci. Model Dev.*, **7**, 531–543, doi:[10.5194/gmd-7-531-2014](https://doi.org/10.5194/gmd-7-531-2014).
- Zhao, Z., and D. Giannakis, 2014: Analog forecasting with dynamics-adapted kernels. *Nonlinearity*, **29**, 2888–2939, doi:[10.1088/0951-7715/29/9/2888](https://doi.org/10.1088/0951-7715/29/9/2888).